TABLE OF CONTENTS – CHAPTER 4

CHAPTER 4
RATIONALE FOR DESIGN OPTION SELECTION

This chapter will document the rationale for the selection of the main design options for the two IFE reactor design studies. As stated in the study objectives, the study team was empowered to seek innovative approaches that would offer increased safety, performance, and economic attractiveness. Many of these factors were quantified and trade studies were employed to make fact-based decisions. Other decisions were predicated upon the more qualitative factors that were stressed as important to the success of fusion as a future energy source.

Another factor that determined why certain key design options were selected depends upon the technology basis assumed. Naturally, state-of-the-art hardware, software, materials, and designs would be employed for systems to be built in the near time frame, but these design studies assumed not today's technology, not tomorrow's technology, but technology some 20 years or more in the future. The project was trying to be visionary as to the future of the applicable technologies. To assure the credibility of the technology extrapolation, results of promising, evolving technologies were founded upon today's experimental evidence, computer modeling, and expert opinion.

The results of the trade studies indicated a specific choice that was easy to select. Other times, the results were not so clear. This is especially true given the clarity of the looking glass into the future. When a choice was particularly difficult, the team opted to choose the more innovative option. Not only was this the charter to follow, but this choice would afford the opportunity for the technical community to examine this option in more detail and consider the merits of future development and examination.

4.1 Selection of Reactor System Technology Options

An inertial fusion power plant involves several major systems including reactor plant, driver, target plant, and balance of plant. The rationale for choosing design options for these major systems involved complicated trade-offs between many issues including economics, safety, engineering feasibility, technical risk, etc. In many instances, design choices were made without considering the impact on the overall system performance. However it was useful (and sometimes essential) to consider an overall figure of merit when selecting design options. The Inertial Confinement systems performance and COst MOdel (ICCOMO) was updated to assist the design process in such instances. This code has evolved over many years. The models were originally developed as part of the STARFIRE reactor design study[1] and were adapted to IFE as part of the HIFSA project.[2] The code contains parametric scaling and cost models for all major power plant subsystems and design options and, as such, it evolved along with the design. It includes KrF laser and heavy ion LINAC drivers, reactor cavity systems, main heat transport systems, target energetics, target manufacturing plant, fuel stream and waste processing, and all balance-of-plant systems.

A key aspect of the systems modeling involves the assessment of projected performance and cost of subsystems that, in many cases, employ technologies at vastly different stages of development. In developing the code, the cost projections were normalized to an equivalent state of engineering maturity across subsystems. This was difficult where comparable hardware does not exist today. Costs were normalized to assumptions made for recent MFE reactor and technology studies[3,4] to provide a common basis for comparison. Elsewhere, costs were based on the best judgment of experts. All cost models were normalized to first production unit costs and updated to conform with the economic guidelines discussed in Section 3. A detailed description of the final cost models is presented in Appendix C.

The study guidelines recommended that costs be developed for a tenth-of-a-kind power plant. However, technology development will not be dictated by projected tenth-of-a-kind costs but rather by those for the first production unit. The trade studies presented in this section thus include no learning curve adjustments. They consider only first production unit costs. Most results are therefore presented in the form of relative comparisons in order to avoid confusion in relating them to the tenth-of-a-kind costs discussed elsewhere in this report.

4.1.1 Laser System Option Selection - The Prometheus-L design point is an outgrowth of a number of different trade studies. These studies are summarized in Table 4.1.1-1. Many design options were evaluated within individual subsystems;

Table 4.1.1-1. Summary of Design Options Considered for KrF Laser System

Parameter	Baseline Value	Options/Range Considered
Target:		
Type	Direct Drive	Indirect Drive
Gain Curves*	Constant Spot	Optimistic, Conservative
Gain Curves	Constant Spot	Zoomed Spot
Number Beams*	60	30-90
Illumination	Tangential Focus	Nested Focus
Incident Energy (MJ)*	4	2-8
Reactor Cavity:		
Wall Protection	Wetted Wall (Lead)	Dry Wall with Fill Gas
Breeder	Li_2O	FLiBe; LiPb Eutectic
Thermal Cycle (He Coolant)	Advanced Rankine	Direct Brayton
Coolant Pressure (MPa)	1.5	1-5
Driver System:		
Laser Amplifier	Electric Discharge w/Raman Accumulator	Large Area E-Beam Pumped
Pulse Compression	Stimulated Brillouin Cell	Angular Multiplex, Hybrid
Amplifier Energy (kJ)*	5.6	3-10
Amplifier Run Time (ns)	250	200-500
Optical Fluence (J/cm^2)*	10	3-10
Final Mirror:		
Type	Grazing Incidence Metal on Ceramic Structure	Grazing Incidence Metal on Metallic Structure
Protection	Distance; Residual Gas; Deflection Magnets	Shutters; Cover Gas; Gas Prism

* The results of this trade study are presented in Section 6.2

however, some selections could not be quantified within a subsystem. The systems code was used to resolve these choices. The discussion presented in this section concerns itself only with the rationale for choosing between technology options, e.g., indirect versus direct drive targets, single versus multiple beam LINAC, etc. The trade studies directed toward selection of an operating range in parameter space for the baseline technology options are discussed in Section 6.2 as noted in the table.

Gain curves for the present study were provided by a DOE-appointed Target Working Group (TWG). The TWG endeavored to level the technical optimism between the various laser illumination concepts (direct drive constant spot - CS, direct drive zoomed spot - ZS, and indirect drive - ID) and the indirect drive heavy-ion targets. For the laser driver, they provided their results in the form of upper and lower bounds on the expected gain as a function of incident driver energy for each option. The TWG recommended an arithmetic mean of the upper bound (optimistic) and lower bound (conservative) as a baseline gain curve for system studies. Figure 4.1.1-1 compares the reference gain curves for direct and indirect drive targets using a KrF laser-driver. These gain curves formed the basis for target design options. The position of the ignition cliff ~2 MJ determines the minimum driver size, and the slope of the curves determines the attractiveness of going to higher driver energy to improve ηG.

Driver performance characteristics are also an important factor in the trade studies. The Prometheus-L driver design is based on the use of non-linear optics (NLO) to improve beam quality and system reliability. Detailed analyses and rationale supporting the design are presented in Section 4.2. A brief overview of the design is presented here to illustrate how it is represented in the systems code.

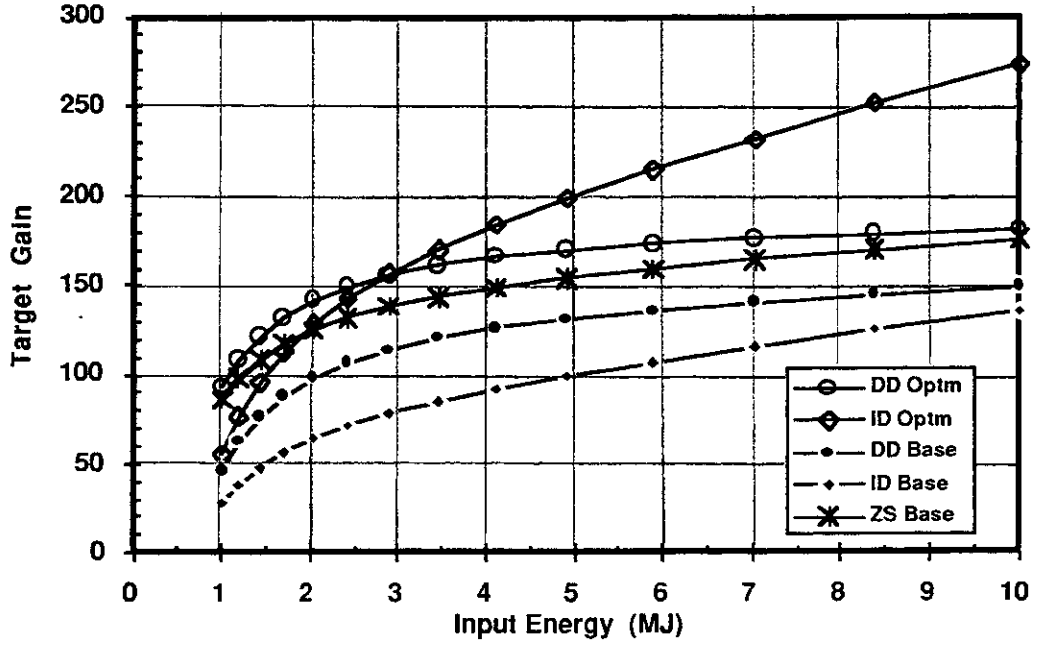

Figure 4.1.1-1. Comparison of Baseline and Optimistic Gain Curves for Direct and Indirect Drive Targets. Direct Drive Curves Assume Constant Focal Spot

The general driver architecture for one of the 60 beamlines is illustrated schematically in Figure 4.1.1-2. It consists of crossed Raman accumulators optically pumped by sixteen 5.9 kJ discharge lasers arrayed four to a side. A Stokes seed is generated for the Raman extraction by splitting off ~1% of the energy from each discharge laser and passing it through a spatially filtered Raman oscillator. The beams are then combined to form a spatially smooth seed that is spectrally and temporally matched to the pumps for maximum extraction efficiency. In addition, the crossed beam geometry serves to smooth out intensity fluctuations across the Raman output aperture. The low quality beams from the discharge lasers are thereby combined to form 60 high brightness beams with very uniform spatial intensity. This permits the downstream optics to operate at higher optical fluence levels (~10 J/cm^2) because local intensity peaking effects are minimal. Simulation studies of such cells by TRW indicate that more than 90% of the discharge laser energy can be Raman converted to the output Stokes beam as discussed in Section 4.2.

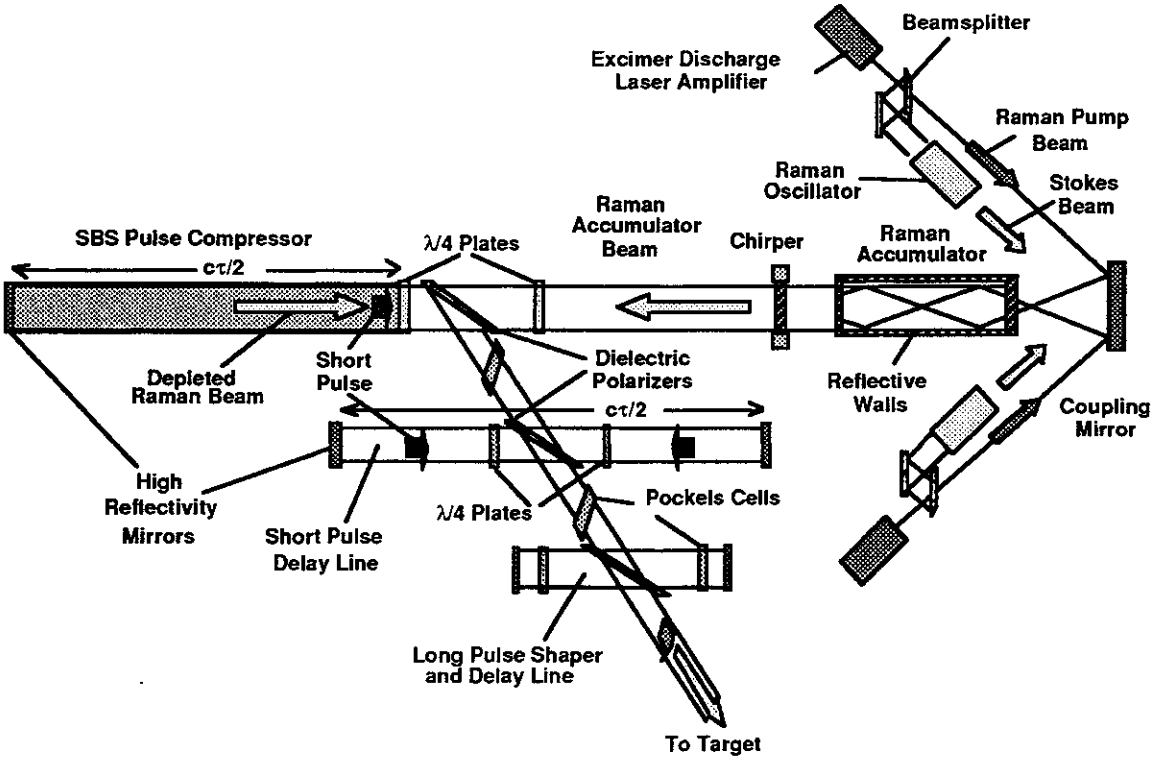

Figure 4.1.1-2. Laser System Architecture for Prometheus-L Driver Design

The output from each Raman accumulator then passes through a precisely timed, electro-optical "chirper" which frequency shifts the first ~10 ns of the beam. The beam continues on into a Stimulated Brillouin Scattering (SBS) cell of length cτ/2. The frequency shift of the "chirped" leading edge is designed to match the SBS shift in the SF_6 gain medium that fills the SBS cell. This enables the leading edge to extract energy from the remainder of the beam as it reflects off the end mirrors and travels back through the optically-pumped medium producing a short duration, high intensity

main pulse appropriate for target implosion. Although the quantum efficiency of this SBS extraction is very high (>99%), the energy tends to be concentrated in a sub-nanosecond pulse at the front of the chirped portion unless care is taken to ramp the amount of power that is chirped. This reduces the efficiency of the SBS extraction to ~65%, as discussed in Section 4.2. However, the unconverted energy is not lost, it still resides in the trailing portion of the pulse.

An optical delay line is provided to interchange the leading edge of the pulse with a portion of the trailing edge. This allows the undepleted SBS pump beam energy to be used as the target prepulse. This is accomplished using a large-aperture Pockels cell to vary the polarization of the leading and trailing portions of the pulse. A dielectric polarizer thus reflects the high intensity leading edge into the delay line but passes the undepleted pulse so that it now becomes a prepulse. The length of the delay line, $c\tau/2$, is chosen to match the prepulse duration requirements, τ = 80 ns. The portion of the undepleted pump extending beyond the 80 ns delay is lost, but this contains < 10% of the total energy. An efficiency of 90% is achieved for the combined SBS/delay line system. It should be noted that the resulting prepulse may have the wrong shape for preparing a proper target atmosphere for the main pulse. Additional pulse shaping may be required. One possible approach utilizes three, large aperture fast Pockels cells in an electro-optical switchyard as indicated in Figure 4.1.1-2. This possibility is discussed further in Section 4.2. Such Pockels cells require significant engineering advances over currently available technology due to the short (~10 ns) repetitive switching times.

The systems code represents the Prometheus-L driver in terms of simple scaling relations for component efficiencies and costs. These relationships are summarized in Table 4.1.1-2, and they lead to a projected overall efficiency of ~6.5% for the laser driver system. To help offset this low efficiency, the excimer discharge laser gas waste heat is recovered and used for feedwater heating. This leads to an effective efficiency of ~8.5% for the laser system.

A significant number of high-quality, large size optics are required for the Prometheus-L system. These optics require good surface figure control, low absorption, anti-reflective and high-reflectivity dielectric coatings at ~250 nm. The optics are sized based on the relations indicated in Table 4.1.1-2. Costs for these components are determined using the algorithms summarized in Table 4.1.1-3. These costs are based on estimates which LLNL developed for the LMF facility.[5] Table 4.1.1-4 summarizes the size and quantity of high power optical components for the 4 MJ Prometheus-L design point to illustrate typical optics requirements for the NLO laser architecture. Optics larger than 1 m linear dimension are segmented to reduce their cost. This should have little effect on performance because a minimum coherent aperture of ~0.5 m is maintained.

Table 4.1.1-2. Laser System Scaling Summary

Item	Effcy/Pwr Rqmt	Sizing Relationship	Cost Relationship (M$)
Front End Systems	Not specifically		
MO and Encoders	accounted for		2.0
Discharge Front End			0.2 N_{DL} E_{DL} / G_{DL}
Discharge Pre-Amps			0.02 C_{DL}
Discharge Lasers	95%*	l = 2 m	
Cavities	15%	w, h based on 3 J/cm^2	0.02 N_{DL} (E_{DL} / 4)$^{0.75}$
E-Beams			0.02 N_{DL} (E_{DL} / 4)$^{0.75}$
Guide Magnets		3 per group, N_{BL} groups	0.209 N_{BL}
Raman Accumulator	96%**	l = 5 m	
Cells	90%	w, h Based on 5 GW/cm	0.01 N_{BL}
Stokes Front End		limit on (intensity *x* length)	0.1 N_{BL}
Stimulated Brillouin	96%**	l = $c\tau$/2	
Cells	90%	10 J/cm^2	0.03 N_{BL}
Chirper System			0.01 N_{BL}
Downstream Optics	95%	10 J/cm^2	
Pulsed Power System	64.3%***	2 m Ceramic PF Lines	
Pulsed Power	Scaled based on		0.005 N_{DL} (E_{DL} / η_{DL})
Discharge Pre-Amps	utilization factor		0.02 C_{DL}
Gas Flow System	1.5 MW	One loop with	
Discharge Gas Flow	Scaled based on	intermediate heat	5.31 N_{BL} (P_G / 18 N_{BL})$^{0.75}$
Discharge Pre-Amps	rep rate, clearing	exchanger for each	0.02 C_{DL}
Gas Purification	stack of 4 cavities	beamline	15.0
Alignmt/Control System			2.84 + 0.194 N_{BL}
Diagnostic System			8.52 (N_{DL} / 960)$^{0.75}$
Pockels Cell Control		4 per beamline	0.02 N_{BL} 4
Power Conditioning			0.084 P_D exp(-0.0005 P_D)
Driver Building		Annulus around reactor	\$88 / m^3
Optics Components			See Tables 4.1.1-3 & 4

* Discharge intrinsic efficiency of 15% and gas pumping effectiveness of 95% are assumed.
** Input and output window transmission efficiency of 98% is assumed.
*** Product of: 94% high voltage, 92% energy storage, 90% pulse forming and $\tau / (\tau + 0.64\ \tau_{rise})$.

Table 4.1.1-3. Optics Cost Basis for Prometheus-L Trade Studies

Component	Type	Blank Cost (\$/cm^3)	Finishing Cost (\$/cm^2)	Coating Cost (\$/cm^2)	Thickness (cm)
Flat Mirror	1	0.13	0.50	0.60	d/16
Spherical Mirror	2	0.13	0.50	0.60	d/16
Window	3	0.60	1.00	0.04	d/16
Lens	4	0.60	1.00	0.04	d/8
Beam Splitter	5	0.60	1.00	0.62	d/8
Thick Window	6	0.60	1.00	0.04	d/10
Thick Lens	7	0.60	1.00	0.04	d/10
Grazing Incidence Mirror	8	540	0.25	0	10, 20% dense
Low Quality Mirror	9	0.13	0.25	0.30	d/16

Blank Size: $w = w_o + 4$ $h = h_o + 4$
Finishing/Coating Area: $A = w\,x\,h$ $d = (w^2 + h^2)^{1/2}$
Mount/Stand Cost: 30% of Blank Cost

Table 4.1.1-4. Prometheus-L Design Point Optical Component and Cost Summary

Component	Quantity	Type	Size (w x h, cm)	Cost (M$)
Discharge Amplifier Windows	920 x 2	3	44 x 44	16.07
Discharge Output Turning Mirrors	960	2	90 x 90	18.54
Raman Accumulator Stokes Mirrors	60	2	18 x 18	0.04
Raman Accumulator Input Windows	36 x 60	3	45 x 45	18.92
Pump Beam Secondary Mirrors	40 x 60	9	90 x 49	14.06
Raman Output Windows	4 x 60	6	90 x 90	19.18
Stimulated Brillouin Polarizer Plates	8 x 60	3	41 x 45	3.79
Brillouin 1/4 Wave Plates	4 x 60	3	45 x 45	2.10
Brillouin Chirper Crystals	4 x 60	3	45 x 45	3.00
Brillouin Cell Mirrors	4 x 60	1	45 x 45	0.96
Delay Line Pockels Cells	4 x 60	3	90 x 90	12.82
Delay Line Polarizer Plates	2 x 8 x 60	3	41 x 45	7.57
Delay Line 1/4 Wave Plates	2 x 4 x 60	3	45 x 45	4.21
Delay Line Turning Mirrors	4 x 60	1	90 x 90	4.64
Relay Turning Mirrors	2 x 60	1	97 x 69	0.93
Vacuum Interface Windows	60	3	97 x 69	2.52
Turning/Pinhole Focusing Mirrors	60	1	97 x 69	0.93
Pinhole Collimating Mirrors	60	2	97 x 69	0.93
Target Focusing Mirrors	60	2	97 x 69	0.93
Grazing Incidence Mirrors	60	8	395 x 69	3.60

Baseline Direct Drive Versus Indirect Drive - The resulting comparison between direct and indirect drive targets for the baseline gain curves is illustrated in Figure 4.1.1-3. This figure highlights the strong preference for direct drive predicted by the baseline gain curves supplied by the TWG. The minimum cost of electricity is ~10% higher for indirect drive and the requisite driver energy increases from 4 to 6 MJ. The driver is thus more complex (2160 discharge lasers as compared to 960 for the direct drive case) and costly (~$250M). This is a direct result of the ηG penalty for the baseline indirect-drive gain curve. For the projected Prometheus-L driver efficiency of 6.5%, the 4 MJ direct drive system has an ηG of 8.2 compared to only 7.0 for the 6 MJ indirect drive case. Illumination symmetry requirements complicate the reactor cavity design for direct drive; however, the analyses discussed in the remainder of this section led to the conclusion that for 60 beams, the cost implications of direct drive illumination are not significant. This was further reinforced by TWG guidance that indirect drive illumination, while not symmetric, would also require roughly 60 beams arrayed on two 60° half-angle cones. Direct drive targets were thus selected for the Prometheus-L system design.

Optimistic Direct Drive Versus Indirect Drive - Figure 4.1.1-4 shows how the direct to indirect drive comparison changes for the optimistic gain curves indicated in Figure 4.1.1-1. As expected, the direct drive advantage is significantly reduced for this case, but it is still favored over indirect drive. The driver costs are virtually

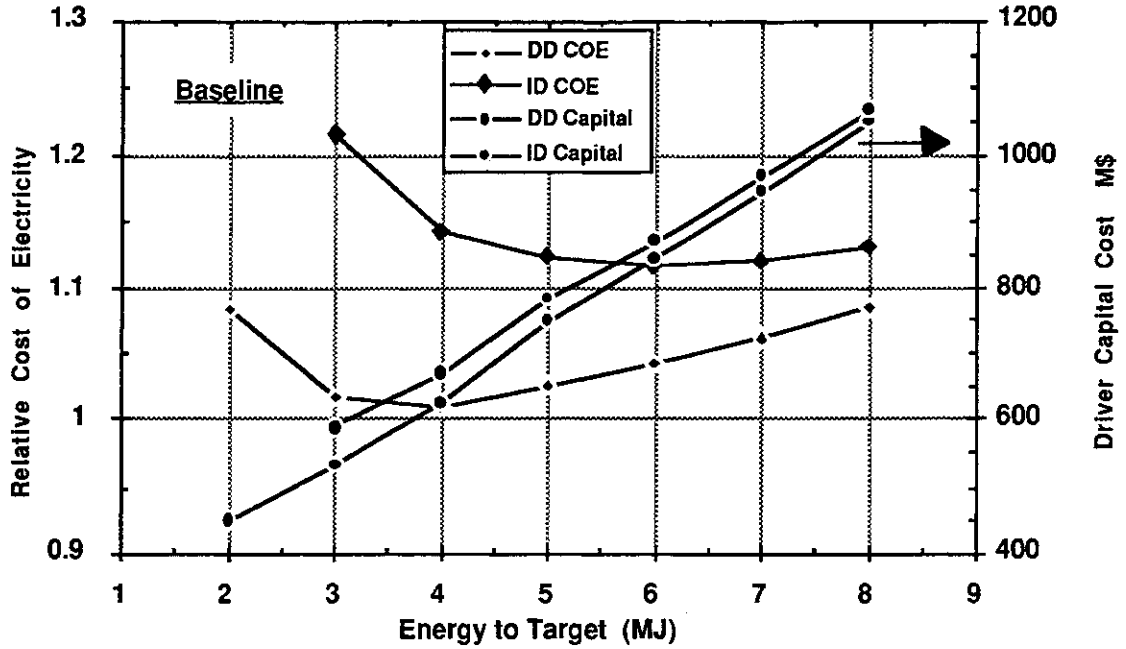

Figure 4.1.1-3. System Performance Comparison for Direct (Solid) and Indirect (Dashed) Drive Targets with Baseline Gain Curves

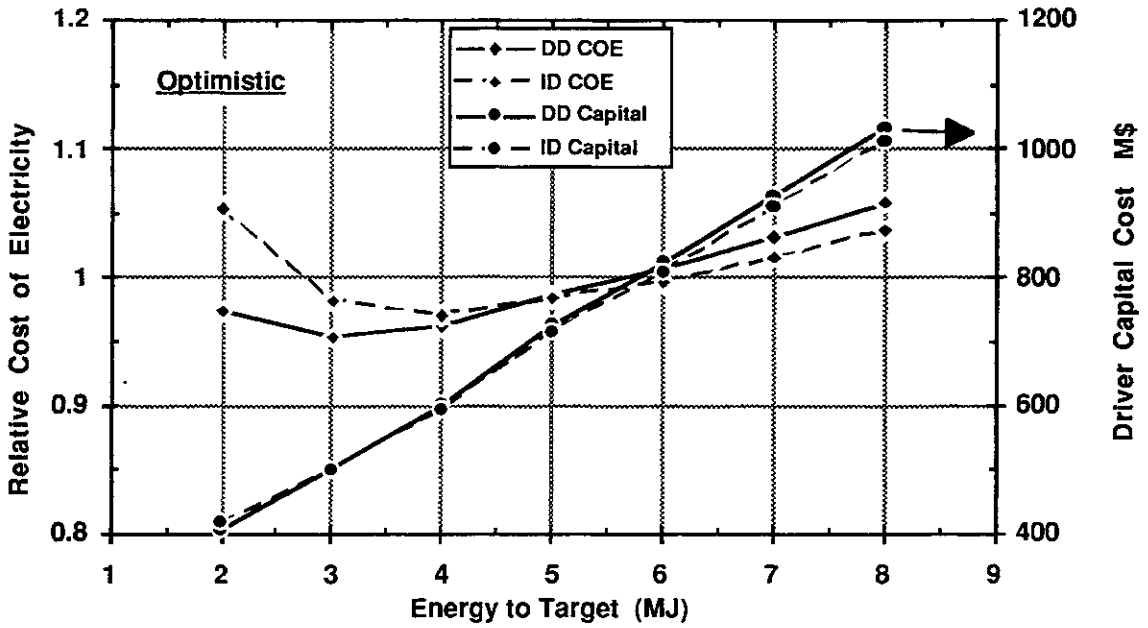

Figure 4.1.1-4. System Performance Comparison for Direct (Solid) and Indirect (Dashed) Drive Targets with Optimistic Gain Curves

identical, but the higher direct-drive gain at low energies leads to a cost advantage for this system. In fact, the minimum indirect drive system cost occurs at 4 MJ even though gain increases significantly beyond that energy. This highlights an important point relative to target design, namely that higher gain is not always beneficial once sufficient ηG has been achieved. The benefit of increasing drive energy depends on the tradeoff between gain curve slope and incremental driver cost. Figure 4.1.1-1 shows that the projected Prometheus-L incremental cost of ~$100/Joule does not favor higher driver energies even if gain scaling is comparable to optimistic expectations.

Constant Spot Versus Zoomed Spot - The final laser design option trade study involves incorporating the capability to zoom the beam focal spot to follow the implosion of the critical energy absorption surface at the target. This leads to higher gain, as indicated in Figure 4.1.1-1, because less energy is wasted in heating the atmosphere around the target, however it complicates the driver design. In order to assess the attractiveness of this possibility, a trade study was conducted with the most optimistic assumption being no added driver cost for zooming. The result of this study is shown in Figure 4.1.1-5. It shows that a zoomed focal spot potentially leads to ~3% lower COE. For the Prometheus NLO laser architecture, the only viable way to zoom the focus involves modifying the rf-driven frequency chirpers for the SBS cells to enable them to introduce a time-varying wavefront curvature. This requires an annular rf field variation around the chirper that significantly complicates its design. The benefit of focal spot zooming was not sufficient to warrant this added complexity. It

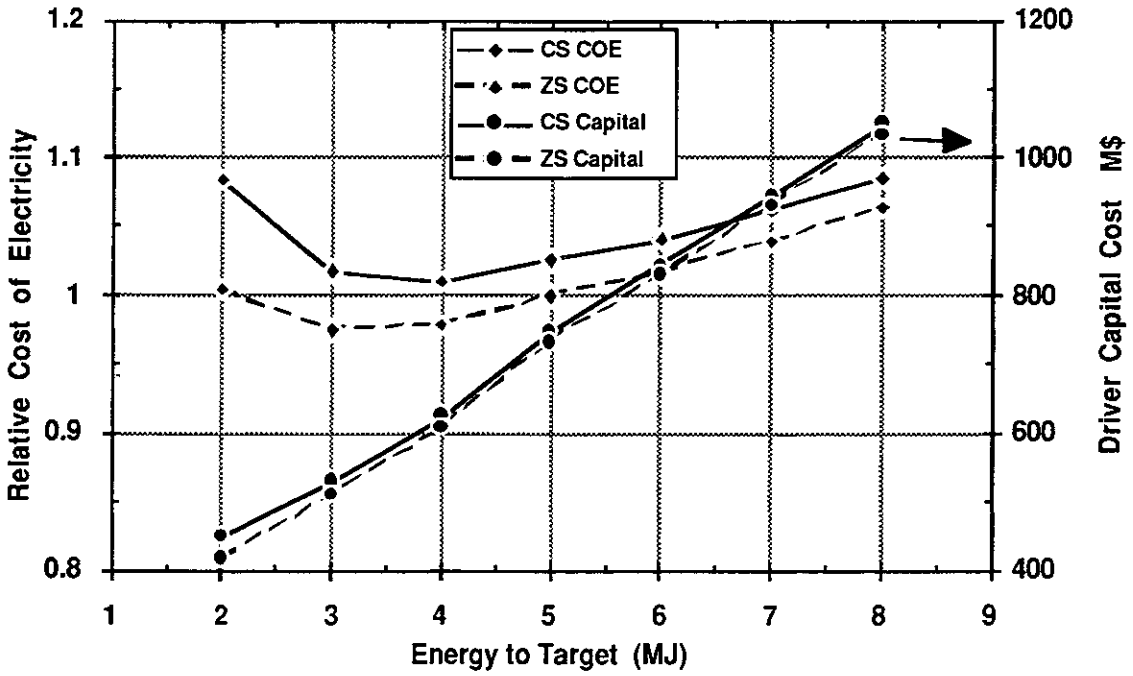

Figure 4.1.1-5. System Performance Comparison for Constant (Solid) and Zoomed (Dashed) Spot Gain Curves

should be noted, however, that the NLO laser architecture provides sufficient beam quality to allow nesting trapezoidally apodized beam focal spots on the target as opposed to the baseline tangential focus option. This possibility, which is discussed in more detail in Section 4.6, may provide the benefit of focal spot zooming without the complications of adding time-varying wavefront curvature.

4.1.2 Heavy Ion System Design Option Selection - The Prometheus-H design point is also based on a number of different trade studies. These studies are summarized in Table 4.1.2-1.

Table 4.1.2-1. Summary of Design Options Considered for Heavy Ion System

Parameter	Baseline Value	Options/Range Considered
Target:		
Type	Indirect Drive	[No Direct Drive Data]
Ion Range (g/cm^2)	0.045 (4 GeV Lead)	0.025-0.2
Spot Size, Radius (mm)*	3	2-5
Illumination	Two Sided	One Sided
Incident Energy (MJ)*	7	4-9
Transport Efficiency (%)*	90	70-100
Reactor Cavity:	Wetted Wall (Lead)	Same as Laser System
Driver System:		
LINAC Type	Single Beam with Storage Rings	Multiple Beam
LINAC Scaling*	$\alpha = 0.2$; $K = -0.15$	$\alpha = (0.2 - 0.5)$; $K = (-0.2 - 0.0)$
Ion Type*	+2 Lead	+1 to +3 Lead
Ion Energy (GeV)*	4	4-8
Focusing Quads	Superconducting	Normal
Cavity Transport	Self-formed Channel	Ballistic; Pre-formed Channel

* The results of this trade study are presented in Section 6.2

The heavy-ion driver has more scaling flexibility because it produces the requisite total energy by combining several ion beamlets at a discrete kinetic energy. The choice of ion charge state and kinetic energy lead to significant differences both in the accelerator configuration and in the target performance that must both be considered in determining the optimum design point. These issues are discussed in Section 6.2.2 along with the results of sensitivity studies which were run to document the leverage of key design parameters indicated in the table on the overall system performance. The discussion presented here focuses on the rationale for choosing a single beam LINAC with intermediate storage rings versus a multiple beam LINAC. The rationale for selecting a self-formed channel for cavity transport and the resulting target focal spot size and channel energy transport efficiency is presented in Section 4.3. Finally, the rationale leading to the choice of a wall protection scheme identical to that for the laser system is presented in Section 4.4, and a discussion of target issues for the heavy ion system is presented in Section 4.6.

Multiple Beam Versus Single Beam - One of the main induction LINAC design challenges involves the space charge limit on transportable current in a periodic focusing lattice. This limit requires multiple transport channels (typically >10 beamlets)

for heavy ion fusion drivers. Past studies[2] have envisioned a multiple beamlet transport lattice consisting of a closely packed quadrupole bundle surrounded by massive induction cores for inertial fusion drivers. The Prometheus-H design considers an alternative approach consisting of a single beam transport lattice coupled with intermediate storage rings to accumulate the required number of beamlets. The approaches are illustrated schematically in Figure 4.1.2-1. This figure highlights the key potential advantages of the single beam system, namely that the accelerator hardware that surrounds the beam(s) (i.e., induction cores, insulator rings, structure and the focusing magnets themselves) are smaller, less complex, and consequently less costly for the single beam system. This simplification, however, is accomplished at the expense of system efficiency which is lower for the single beam approach. The induction cores must be cycled many times (once for each beamlet) to produce each main pulse as compared to one cycle for each main pulse in the multiple beam case. The systems code was used to quantify this tradeoff.

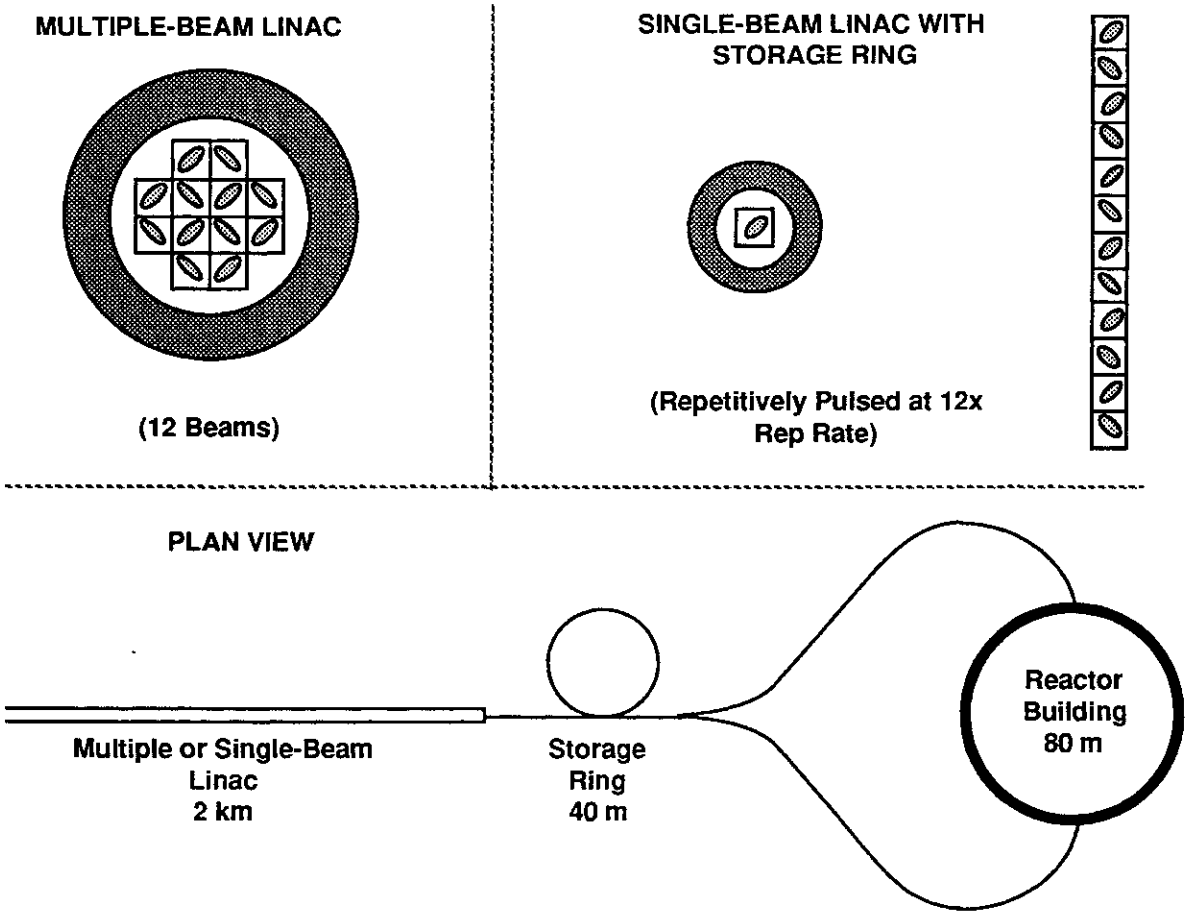

Figure 4.1.2-1. Comparison of Multiple and Single Beam LINAC Configuration

The systems code modeling is based on the general relations summarized in Table 4.1.2-2. The LINAC is sized assuming a maximum accelerating gradient of 1 MV/m. Focusing magnet quantities are determined using continuous limit focal lattice scaling laws developed by Maschke[6]. These scaling relations are summarized in Section 6.2. Injector costs (ion source plus acceleration up to 3 MV) are assumed to be $10M per injector for a single beam system. Multiple beam systems are assumed to require four such injectors. Insulator and accelerator structure costs are calculated based on the final column voltage, V_F, and inner core radius, R_{Ci}, from estimates LBL developed for a 0.83 m radius multiple-beam LINAC.

Table 4.1.2-2. Heavy-Ion System Scaling Summary

Item	Effcy/Pwr Rqmt	Qty/Sizing Relationship	Cost Relationship (K$)
Injector	3 MeV	1 SB; 4 MB	10,000 per injector
Linear Accelerator		Length based on 1 MV/m	
Insulator		Radius scaled with R_{Ci}	10 V_F (R_{Ci} / 0.83)
Structure		from 0.83 m reference	8.76 V_F (R_{Ci} / 0.83)
Induction Core	V_{Core} (J/m^3) N_{Bmlet}	Scaled with G, τ, ΔB, R_{Ci}	32 V_{Core}; $5 / kg
Focusing Magnets		Based on lattice scaling	(55 + 10 N_W + 5 L_M) N_M f_{LC}
Cryogenic System	1000 W_{Cold}	W_{Cold} = N_M (3 W/mag)	4 W_{Cold}
Vacuum System		Scaled with length	5.08 L_{Acc}
Storage Rings		1 per beamlet*	
Magnets		Based on lattice/bending	(55 + 10 N_W + 5 L_M) N_M f_{LC}
Cryogenic System	1000 W_{Cold}	W_{Cold} = N_M (3 W/mag)	4 W_{Cold}
Vacuum System		Scaled with length	5.08 L_{SR}
Final Transport		Main beamlets + prepulse**	
Buncher	2 MB LINACs	Based on bunching rqmts	Same as main LINAC
Drift Section		2 sides, 180 m long	
Magnets		Based on lattice scaling	(55 + 10 N_W + 5 L_M) N_M f_{LC}
Cryogenic System	1000 W_{Cold}	W_{Cold} = N_M (3 W/mag)	4 W_{Cold}
Vacuum System		Scaled with length	5.08 L_{FT}
Pulsed Power	60%***	Core loss + Beam energy	10 / kJ****
Instrument & Control			0.05 C_{Tot}
Auxiliary Systems			0.02 C_{Tot}
Beamline Tunnel		W_{Tun} = 5.0 R_{Co}	$120 / ft^2
PFN Building		0.5 W_{Tun}	$50 / ft^2

* Each main pulse beamlet has its own storage ring, prepulse beamlets are grouped in two rings
** Main pulse beamlets are bundled into one buncher, two prepulse beams in the other
*** Product of 70.6% for high voltage and energy storage and 85% for pulse shaping
**** Pulsed power costs are increased by a factor of 10 for the single beam system

Induction cores are sized based on R_{Ci} and the product of acceleration gradient, G, and pulse length, τ, at each point along the LINAC. The core radius is chosen so that it clears the outer radius of the quadrupole bundle as depicted in Figure 4.1.2-1. Core losses in J/m^3 are determined using the loss curve shown in Figure 4.1.2-2. The figure

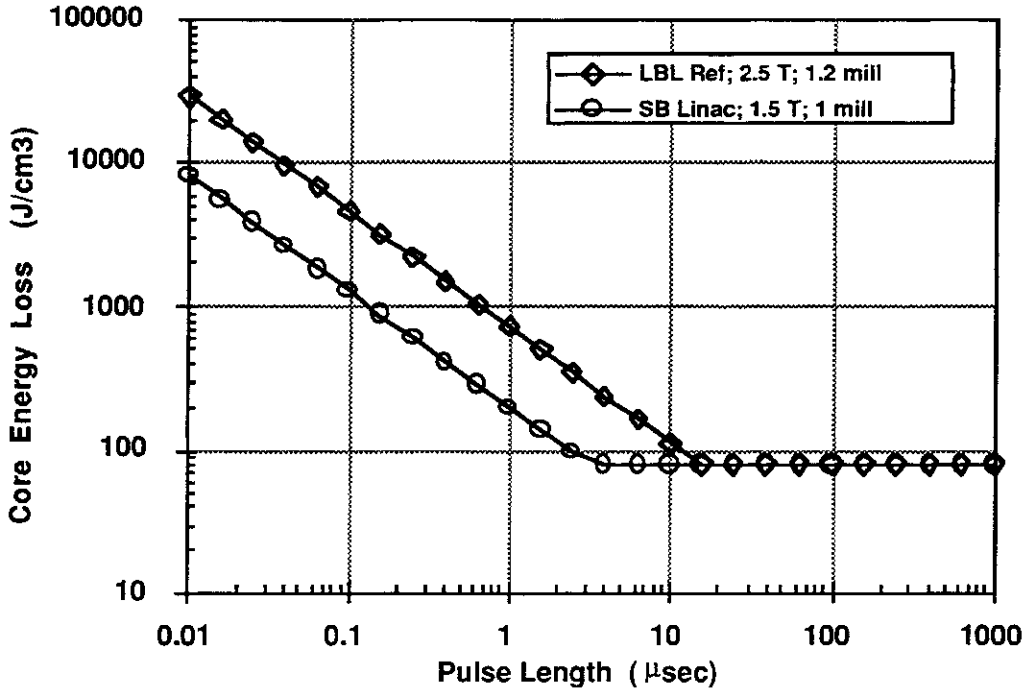

Figure 4.1.2-2. Assumed Metglas Loss Scaling with Pulse Length for LINAC System Studies

depicts the measured losses for a flux swing $\Delta B = 2.5$ T and a winding thickness $t = 1.2$ mills. These are scaled to the lower curve using the relation

$$\text{Core Losses} = \text{Core Losses}_o \left(\frac{\Delta B}{\Delta B_o}\right)^{1.8} \left(\frac{t}{t_o}\right)^2$$

for the flux swing of 1.5 T and winding thickness of 1 mill assumed here. For the single beam system, core losses are multiplied by the number of beamlets, N_{Bmlet}, to account for recycling. Core costs are estimated using \$5 per kilogram of Metglas. An 80% packing fraction is assumed in calculating the core volume. Pulsed power requirements are determined based on the sum of the core losses and the energy gained by the beam. Costs for pulsed power are estimated at \$10 per joule for the multiple beam system and \$100 per joule for the single beam case. These costs are based on information provided by LBL for the multiple beam system[7] and LLNL for the rapidly cycled (10's of kHz) single beam system. The factor of 10 increase recommended for the single beam case is based on recent LLNL work on recirculating LINAC systems.[8]

Magnet costs are based on data for similar quadrupoles for the Superconducting Super-Collider. This indicates that each cryostat will cost \$55,000 with an additional \$10,000 for each quadrupole winding plus \$5000 per meter of length. These costs are adjusted using an 85% learning curve factor, f_{LC}, to determine the magnet costs for the "first production" driver considered here. Cryogenic system costs are based on the

total number of magnets per section, including quadrupoles and dipoles, N_M, with a heat leak of 3 watts per magnet. A cost of $4000 per cold watt, W_{Cold}, is assumed with a power consumption of 1 kW per cold watt. Vacuum system costs are estimated at $5100 per meter of length for each section and tunnel costs at $120 per square foot. The tunnel width is taken to be five times the maximum core outer radius R_{Co}. Finally, I&C and auxiliary systems are assumed to be 5% and 2% respectively of the total cost.

The resulting comparison between projected system performance for the multiple and single beam LINAC drivers is illustrated in Figure 4.1.2-3. This comparison uses lattice scaling suggested by Ed Lee[9], since it was thought to be most favorable for multiple beam systems. The final single beam design uses an alternative lattice scaling discussed in Section 6.2 and therefore has lower capital cost than those presented here. Nevertheless, this figure still highlights the significant advantage projected for the single-beam approach in spite of its lower efficiency (15% as compared to 37%). Driver capital costs for the single beam system are roughly half those for the multiple beam system and this leads to a 12% reduction in COE. The single beam system was therefore selected for the baseline driver in the Prometheus-H design study.

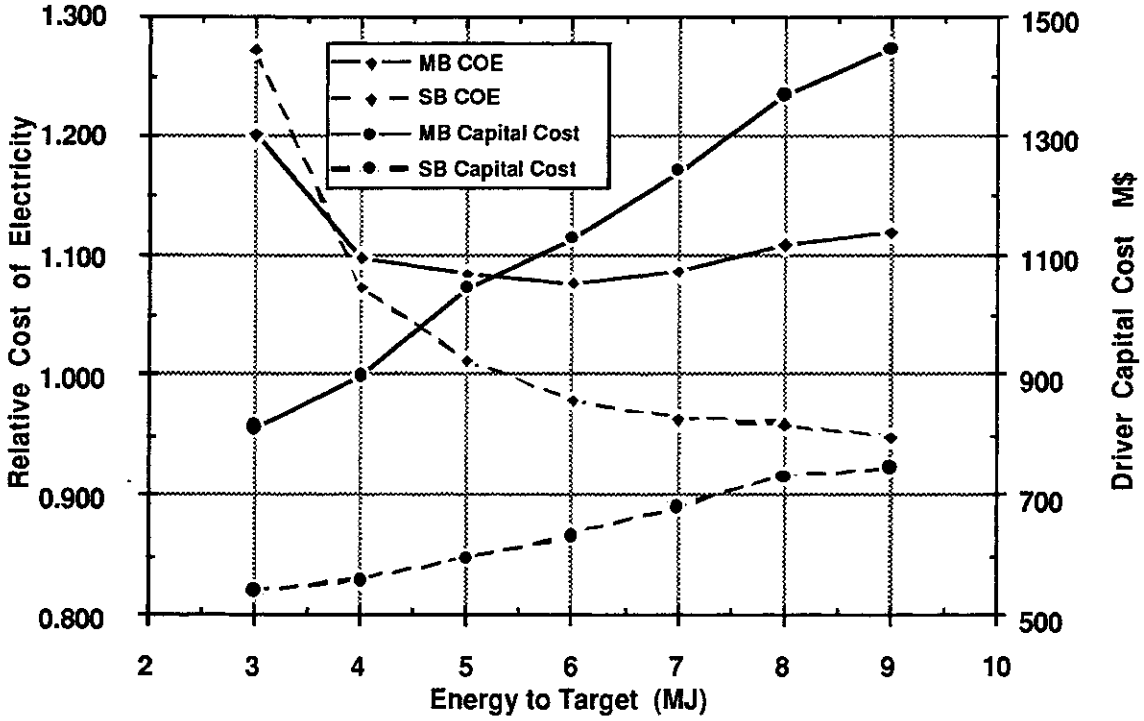

Figure 4.1.2-3. Comparison of Projected COE and Driver Capital Cost for Multiple and Single Beam LINACs. Systems are all 4 GeV, +2 Lead with 3 mm Radius Focal Spot.

It should be noted, however, that the multiple-beam system remains a viable driver option. Its COE is comparable to that for the KrF laser system, and the alternative transport lattice scaling discussed in Section 6.2 leads to significantly lower MB capital costs than those presented here. In addition, it avoids technical issues associated with beam stability and particle loss in the storage rings. These are critical R&D concerns for the single beam approach and they are highlighted in Section 5.

In spite of these concerns the Prometheus-H design point represents a tantalizing development goal. The single beam configuration dramatically lowers the driver cost and technology development challenge while still providing sufficient ηG for an attractive overall system. Furthermore, the 4 GeV ion energy is more attractive to target designers due to its reduced range. Significant issues need to be resolved concerning the storage rings but the starting point is much more appealing than any previously envisioned for induction LINAC drivers.

References for 4.1

1. C. C. Baker, M. A. Abdou, et al., "STARFIRE - A Commercial Tokamak Fusion Power Plant Study," ANL/FPP-80-1, September 1980.

2. D. S. Zuckerman, et al., "Induction LINAC Driven Heavy Ion Fusion System Model," Fusion Technology, Vol. 13, #2, 1986.

3. R. L. Miller, "Options and Optimizations for Tokamak Reactors: ARIES, " 9th Topical Meeting on Technology of Fusion Energy (Oakbrook, Illinois, 7-11 October 1990)

4. Ronald L. Miller, Robert A. Krakowski, David A. Ehst, ARIES System Study Results (Draft), 15 February 1991.

5. D.B. Harris, et al., KrF Laser Driven Laboratory Microfusion Facility Conceptual Design Report," LANL Report LA-UR-91-2915, December 17, 1991.

6. Mr. Alfred Maschke, TRW, Personal Communication, 1991.

7. Unpublished cost analyses performed for LBL HI LMF conceptual design, c.f. Ref 9.

8. J.J. Barnard, et. al., "Study of Recirculating Induction Accelerators as Drivers for Heavy Ion Fusion," LLNL Report UCRL-LR-108095, September 21, 1991

9. Edward P. Lee, et.al., "Heavy Ion Driven LMF Design Concept," LBL Report LBL-31-248, August 1991.